

Energy transport and scintillation of cerium-doped elpasolite $\text{Cs}_2\text{LiYCl}_6$: Hybrid density functional calculations

Koushik Biswas and Mao-Hua Du*

*Materials Science & Technology Division and Center for Radiation Detection Materials and Systems,
Oak Ridge National Laboratory, Oak Ridge, Tennessee 37831, USA*

(Received 4 May 2012; published 5 July 2012)

Elpasolites are a large family of halides that have recently attracted considerable interest for their potential applications in room-temperature radiation detection. $\text{Cs}_2\text{LiYCl}_6$ is one of the most widely studied elpasolite scintillators. In this paper, we show hybrid density functional calculations for electronic structure, energetics of small polarons and self-trapped excitons, and excitation of luminescence centers (Ce impurities) in $\text{Cs}_2\text{LiYCl}_6$. The results provide important understanding of energy transport and scintillation mechanisms in $\text{Cs}_2\text{LiYCl}_6$ and other rare-earth elpasolites.

DOI: [10.1103/PhysRevB.86.014102](https://doi.org/10.1103/PhysRevB.86.014102)

PACS number(s): 71.35.Aa, 71.38.Ht, 71.55.—i

I. INTRODUCTION

Scintillators are an important class of materials that can emit light when excited by radiation. This property leads to the use of scintillators as means of detecting x- and γ -rays and neutrons. Scintillator materials are widely used today in areas such as nonproliferation of special nuclear materials, homeland security, medical imaging, and high-energy physics.¹ Scintillators are also used to generate light in fluorescence tubes.

A scintillator material can absorb radiation energy through the excitation of electrons and holes. These electrons and holes can recombine and emit photons. Efficient scintillation is often facilitated by impurities or so-called activators. This usually requires the diffusion of radiation-generated electrons and holes to the activators, where the radiative recombination occurs. However, competing processes such as nonradiative recombination or trapping at lattice defects may hinder the diffusion of electrons and holes to the activators. Moreover, the free electrons and holes may be unstable against self-trapping, thereby creating polarons and self-trapped excitons (STEs),² whose diffusion depends on their migration barriers. Trapping of electrons and holes at the activators is due to the presence of electronic gap states induced by the activator. In the case of Ce-doped scintillators, the Ce $4f$ and $5d$ levels need to be inside the band gap of the host material to trap holes and electrons, respectively.^{3–5} The emitted photons can be detected and analyzed to obtain the kinetic energy, time, and/or real-space position of radiation events.

There are many desirable properties for a scintillator material, such as high density (for large radiation stopping power), high light output, good energy resolution, fast decay time, and availability of large single crystals. These properties are related to fundamental material properties such as band gap (important for the light output), carrier transport efficiency (relevant to scintillation decay), and optical, chemical, and structural properties. The demand for new scintillator materials with improved properties requires understanding of the electronic structure and the scintillation mechanisms of the materials. In this paper, we show first-principles calculations for a range of material properties relevant to scintillation for a prototypical elpasolite compound, $\text{Cs}_2\text{LiYCl}_6$. The goal is to provide

understanding of the scintillation mechanisms and assist in the search for new scintillator materials within elpasolites and other classes of materials.

Elpasolites are a large family of halides that have recently attracted considerable interest for radiation detection applications.^{6–19} The general formula of elpasolites is $A_2^+B^+B'^{3+}X_6^-$ (Fig. 1). Here X^- is a halogen ion (F, Cl, Br, or I). A^+ and B^+ are typically (but not limited to) alkali metal ions. B'^{3+} can be a rare-earth, transition metal, or other trivalent ion. It can be quickly seen that there are hundreds of elpasolites.²⁰ Elpasolites are attractive as scintillators because (1) a large number of them are cubic (double-perovskite structure), ideal for crystal growth from melt; (2) the B' site is well suited for the doping of Ce^{3+} , whose $5d$ and $4f$ states can trap electrons and holes for radiative recombination; (3) the large number of elements that can be incorporated into them offers the opportunity to find desired material properties for scintillation applications; and (4) besides γ -ray detection, the neutron detection is possible when neutron-conversion elements are incorporated (e.g., ^6Li on the B site).

$\text{Cs}_2\text{LiYCl}_6$ is one of the most widely studied elpasolite compounds for its potential capability for neutron detection.^{6–10} $\text{Cs}_2\text{LiYCl}_6$ has a modest γ -light output of 20 000 photons/meV and a slow scintillation decay time of several microseconds.^{6,8,16} The slow scintillation decay was attributed to the formation of STEs and their slow energy transfer to Ce^{3+} .³ Electron paramagnetic resonance studies on $\text{Cs}_2\text{NaYCl}_6$ found both hole and electron polarons,²¹ indicating the localized nature of both the valence and the conduction band states. Optical measurements on $\text{Cs}_2\text{LiYCl}_6$ revealed significant absorption of STE emission by Ce, indicating that STEs have low mobility and that radiative energy transfer plays an important role in energy transfer from STEs to Ce.^{3,16,17} Among halides with common cations, hole mobility typically increases from chlorides to bromides (due to the more delocalized valence band states in bromides) and thus should result in faster carrier transport and scintillation. Indeed, scintillation decay in $\text{Cs}_2\text{LiYBr}_6$ is faster than in $\text{Cs}_2\text{LiYCl}_6$ but still has a slow component of several microseconds.¹⁶ In contrast, LaBr_3 , also a bromide, is a fast scintillator with a scintillation decay time of a few tens of nanoseconds.²² To study the scintillation response, it is important to understand the electronic structure

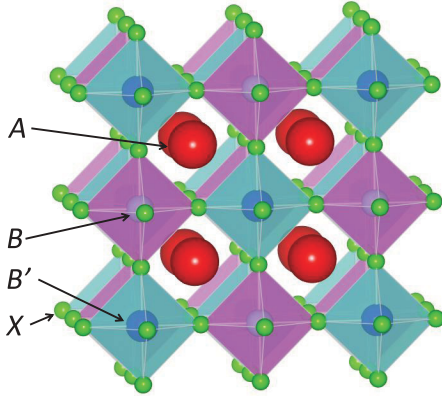


FIG. 1. (Color online) Structure of an elpasolite compound ($A_2BB'X_6$).

and carrier transport in the scintillator. In this paper, we present results on electronic structure, energetics of polarons and STEs, and properties of Ce activators in Cs_2LiYCl_6 and discuss their impact on energy transport.

II. METHODS

Our calculations are based on the hybrid density functional method as implemented in the Vienna *ab initio* simulation package.^{23,24} Perdew-Ernzerhof-Burke hybrid functionals (PBE0),²⁵ which have a 25% Hartree-Fock exchange, were used in the calculations.²⁶ The calculations using Heyd-Scuseria-Ernzerhof (HSE) functionals,^{27,28} which include short-range exchange screening, were also performed on the Ce impurity properties for comparison with the PBE0 results. The screening parameter of the nonlocal Fock exchange in the HSE calculations was set at 0.2 \AA^{-1} (the HSE06 functional).²⁸ The hybrid density functional methods have been shown to improve results on the band gap, defects, and charge localization in semiconductors.^{29–32}

The electron-ion interactions were described using projector augmented wave potentials.^{33,34} The valence wavefunctions were expanded on a plane-wave basis with a cutoff energy of 280 eV. A 40-atom cubic supercell was used in the calculations. A $2 \times 2 \times 2$ grid was used for the k-point sampling of Brillouin zone. All atoms were relaxed to minimize the Feynman-Hellmann forces to below 0.05 eV/\AA . The experimental lattice constant of 10.4857 \AA ³⁵ was used in both PBE0 and HSE06 calculations.

The charge transition level $\varepsilon(q/q')$, induced by Ce impurity or polarons, is determined by the Fermi level (ε_f) at which the formation energies of the impurity or defect with charge states q and q' are equal to each other. $\varepsilon(q/q')$ can be calculated using

$$\varepsilon(q/q') = \frac{E_{D,q'} - E_{D,q}}{q - q'}, \quad (1)$$

where $E_{D,q}$ ($E_{D,q'}$) is the total energy of the supercell that contains the relaxed structure of a defect at charge state q (q').

The binding energies of hole and electron polarons (or the energies of hole and electron polarons relative to those of free hole and free electron) are $\varepsilon_{\text{hole-pol}}(+/0) - \varepsilon_V$ and $\varepsilon_C - \varepsilon_{\text{electron-pol}}(0/-)$, respectively. Here, ε_V and ε_C are the energies of the valence band maximum (VBM) and the

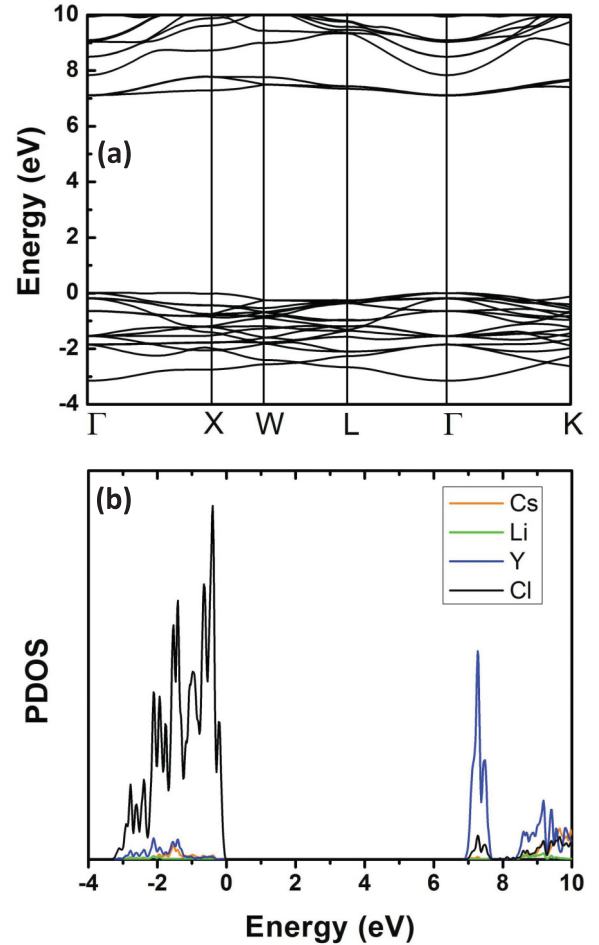


FIG. 2. (Color online) (a) Band structure and (b) PDOS of Cs_2LiYCl_6 . The energy of the valence band maximum is set to zero.

conduction band minimum (CBM), respectively. $\varepsilon_{\text{hole-pol}}(+/0)$ and $\varepsilon_{\text{electron-pol}}(0/-)$ are the transition levels for the hole and the electron polarons, respectively, calculated using Eq. (1). A polaron exists only when there is a localized charge. When calculating transition levels for polarons using Eq. (1), the structure for the neutral charge state is simply that for the defect-free host material. Therefore, the binding energies of hole and electron polarons are $E_0 - E_{\text{hole-pol}} - \varepsilon_V$ and $\varepsilon_C - E_{\text{electron-pol}} + E_0$, where E_0 is the energy of the neutral defect-free supercell and $E_{\text{hole-pol}}$ and $E_{\text{electron-pol}}$ are the energies of the supercells that contain relaxed structures of hole and electron polarons, respectively.

We checked the convergence of the results with respect to the supercell size by calculating the hole polaron binding energy in a larger (80-atom) face-centered cubic supercell. The resulted hole polaron binding energy is higher by 0.07 eV than that using 40-atom supercells. This small energy change indicates that the small polaron is highly localized and that a small 40-atom supercell can yield reasonable results.

III. RESULTS AND DISCUSSION

A. Electronic structure

Figure 2(a) shows the band structure of Cs_2LiYCl_6 . It can be seen that Cs_2LiYCl_6 has a direct band gap at the Γ

point. The calculated band gap is 7.08 eV, in good agreement with the experimentally estimated value of 7.5 eV.¹⁷ The site-projected density of states for Cs₂LiYCl₆ [Fig. 2(b)] shows that the conduction and valence band edge states are derived from Y-4*d* and Cl-3*p* states, respectively, and both have very small dispersion. The small dispersion for the valence band is common in many halides, because the *p*-states of halides are usually relatively localized. As a result, the formation of a halogen–halogen bond associated with the formation of a small polaron (or a V_k center) could lower the total energy more than the energy cost of localizing a hole (about half of the valence band width). This leads to the spontaneous formation of small hole polarons in many halides.^{36,37} However, the narrow conduction band of very small dispersion, as seen in Cs₂LiYCl₆, is unusual. This is in sharp contrast to typical compound semiconductors and insulators, in which the conduction band is usually more dispersive than the valence band—resulting in electron mobility that is higher than hole mobility. Cs₂LiYCl₆ has three cations. Y has the lowest electronegativity among the three cations; thus, the empty 4*d* states of Y³⁺ are the lowest conduction band states. Also, the double-perovskite structure of elpasolites (see Fig. 1) results in a large distance between the two nearest-neighbor *B* or *B'* site ions and hence a small degree of hybridization among *B* or *B'* states. Thus, the small dispersion of the conduction band of Cs₂LiYCl₆ may be understood by a combination of the localized Y-4*d* states and the large nearest-neighbor Y-Y distance of 7.4 Å in Cs₂LiYCl₆.

B. Self-trapped carriers and excitons

Hole self-trapping and the formation of the V_k center are commonly seen in halides due to the localized valence band states and the soft lattice.^{36,37} For Cs₂LiYCl₆, the small dispersion of the conduction band indicates that the electron polaron may also form. Indeed, our first-principles calculations show that both electron and hole polarons are stable. In the hole polaron or the V_k center, two Cl ions move close to each other to form a Cl₂[−] hole center where the unpaired electron is shared between the two Cl ions. The V_k center formed next to an Y ion is calculated to be more stable than that next to a Li ion by 0.28 eV. This is consistent with the experimental result for Cs₂NaYCl₆, which also shows that the V_k center stabilizes next to an Y ion.²¹ Hole self-trapping near an Y ion shortens the Cl-Cl distance to 2.63 Å, which is 1.11 Å shorter than the Cl-Cl distance without a localized hole. In the electron polaron, we find that the electron is localized at an Y ion, which results in the elongation of the Y-Cl bond by 0.11 Å. Self-trapping of a hole and an electron lowers the total energy by 0.50 and 0.43 eV, respectively, which are the binding energies of hole and electron polarons as defined in Sec. II. The electron and hole polarons can further bind to form a triplet STE with a binding energy of 0.41 eV. Therefore, the overall STE binding energy relative to a free hole and a free electron is 1.34 eV, which is the sum of the binding energies of hole and electron polarons (0.50 and 0.43 eV, respectively) plus the STE binding energy relative to a pair of isolated hole and electron polarons (0.41 eV). Figure 3 shows the partial charge density of the localized electron and hole in a STE. Following Franck-Condon principles, STE emission energy

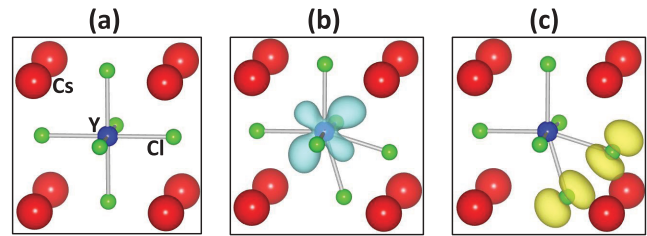


FIG. 3. (Color online) (a) Structure of the undistorted YCl₆ octahedron in Cs₂LiYCl₆; isosurfaces of partial charge densities of (b) the localized electron state and (c) the localized hole state in a STE. The charge densities of the isosurfaces in (b) and (c) are -0.005 and $0.005 e/\text{bohr}^3$, respectively.

is calculated by taking the energy difference between the supercell that contains a STE and the one with the same STE structure but in the electronic ground state. The calculated STE emission energy is 3.90 eV. In comparison, a broad emission band centered at 3.6 eV (full width at half maximum of 1.1 eV at 100 K) was found in x-ray-excited optical luminescence spectra of undoped Cs₂LiYCl₆,¹⁶ in good agreement with the calculated value.

The calculated binding energies of the polarons and the STE are the upper limits of their respective diffusion barriers. The hybrid functional calculations of diffusion barriers for polarons and STEs are time consuming and will be the subject of future study. It is often argued based on alkali halides that the STE diffusion barrier should be lower than that of the hole polaron because the charge neutral STE induces less polarization distortion of the lattice.² However, there are two important differences between alkali halides and Cs₂LiYCl₆: (1) the electron polaron is stable in Cs₂LiYCl₆ but not in alkali halides and (2) the distance between the nearest-neighbor Y ions (where the electron self-traps) in Cs₂LiYCl₆ is long compared to the cation–cation distances in alkali halides. In Cs₂LiYCl₆, the hole polaron forms near an Y ion. When it hops to the nearby Li, the electron polaron on Y cannot hop to Li, because the energy levels of Li are significantly higher than those of Y. Thus, the STE diffusion in Cs₂LiYCl₆ needs to partially overcome the binding energy between the electron and the hole polarons. Only after the hole polaron diffuses to the nearest-neighbor Y site through Y→Li→Y hopping steps can the electron polaron hop to the same nearest-neighbor Y site. Therefore, in Cs₂LiYCl₆, the STE diffusion barrier may not be lower than that of the hole polaron and the STE diffusion is expected to be inefficient.

Experiments suggest that both radiative and nonradiative energy transfer from the excited carriers to Ce occurs in Cs₂LiYCl₆.¹⁶ The temperature-dependent light yield measurement shows that the light yield initially increases with temperature due to the enhanced efficiency of the STE thermal diffusion and then decreases with temperature at higher temperatures (near and above room temperature) due to the nonradiative recombination of the STEs.¹⁶ The emission and excitation spectra show that a large portion of the STE emission is absorbed by Ce,¹⁶ indicating significant radiative energy transfer. The scintillation efficiency appears to be limited by the STE lifetime, which is on the order of microseconds.¹⁶

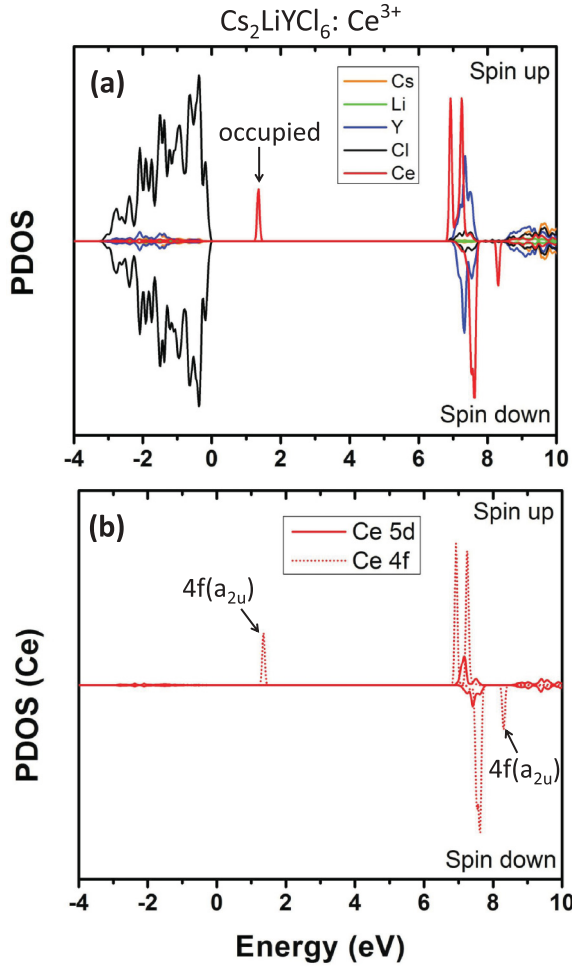


FIG. 4. (Color online) PODS of (a) $\text{Cs}_2\text{LiYCl}_6:\text{Ce}^{3+}$ and (b) the $4f$ and $5d$ states of Ce^{3+} calculated in a $\text{Cs}_8\text{Li}_4\text{Y}_3\text{Cl}_{24}\text{Ce}$ supercell. The energy of the valence band maximum is set to zero.

C. Ce impurity

Ce has an oxidation state of +3 and thus can substitute an Y^{3+} ion in $\text{Cs}_2\text{LiYCl}_6$. The $4f$ and the $5d$ states of Ce^{3+} in $\text{Cs}_2\text{LiYCl}_6$ can capture a hole and an electron, respectively, which subsequently recombine radiatively to emit a photon. Figure 4 shows the partial density of states (PODS) for the ground-state Ce, i.e., Ce^{3+} , in a 40-atom $\text{Cs}_2\text{LiYCl}_6$ supercell. In the cubic structure of $\text{Cs}_2\text{LiYCl}_6$, the Ce $4f$ state is split to a nondegenerate a_{2u} state and threefold degenerate t_{1u} and t_{2u} states, while the $5d$ state is split to a twofold degenerate e_g state and a threefold degenerate t_{2g} state. For the ground-state Ce^{3+} , the singly occupied $4f(a_{2u})$ state is deep inside the band gap, and there is large exchange splitting for the $4f(a_{2u})$ state, as shown in Fig. 4. The Ce $5d$ states are resonant in the conduction band, hybridizing with cation states. Clearly, Ce^{3+} can capture a hole to become Ce^{4+} . In Ce^{4+} , all seven empty $4f$ states and the three empty $5d(t_{2g})$ states are inside the band gap, while the $5d(e_g)$ states resonate in the conduction band, as shown in Fig. 5. An electron can then be trapped at the Ce $5d(t_{2g})$ state to form a $\text{Ce}^{3+,*}$, where the $5d$ - $4f$ emission occurs. The positions of the $4f$ and $5d$ levels of

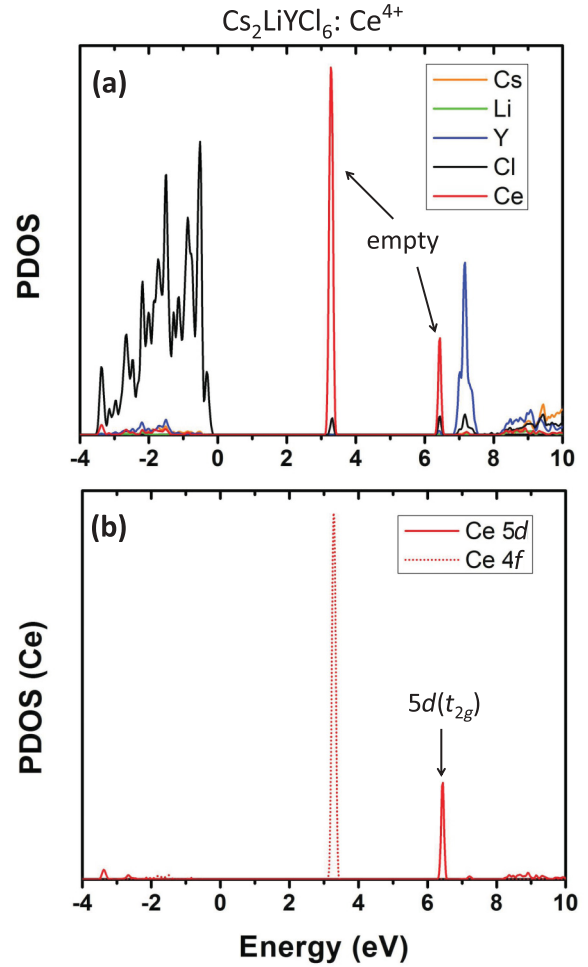


FIG. 5. (Color online) PODS of (a) $\text{Cs}_2\text{LiYCl}_6:\text{Ce}^{4+}$ and (b) the $4f$ and $5d$ states of Ce^{4+} calculated in a $\text{Cs}_8\text{Li}_4\text{Y}_3\text{Cl}_{24}\text{Ce}$ supercell. The energy of the valence band maximum is set to zero.

Ce strongly depend on the electron occupation, reflecting the strong Coulomb interaction. The occupation of the $4f$ level also affects the $5d$ level position due to screening by the $4f$ electrons. Only $4f$ levels of Ce^{3+} are present in the band gap, and the $5d$ states appear inside the band gap only after Ce^{3+} is turned Ce^{4+} by capturing a hole. Therefore, Ce^{3+} must capture a hole before it can capture an electron.

Energy transfer to the scintillation centers may be accomplished by trapping a STE at a Ce ion or consecutive trapping of a hole and an electron polaron, as shown in Eq. (2). This trapping causes the excitation of Ce^{3+} to $\text{Ce}^{3+,*}$. We calculated the trapping energy for a STE, a hole polaron, and an electron polaron at a Ce ion. Trapping of a STE by Ce^{3+} lowers the total energy by 1.89 eV [Eq. (2a)]. Trapping of a hole polaron at Ce^{3+} lowers the energy by 1.69 eV [Eq. (2b)], and subsequent trapping of an electron polaron at Ce^{4+} lowers the energy by 0.61 eV [Eq. (2c)]. Direct trapping of an electron polaron at Ce^{3+} is not favorable, because it incurs an energy cost of 0.21 eV. The trapping energies shown in Eq. (2) are large enough to prevent thermal detrapping of the charge from Ce at room temperature, which can suppress luminescence.

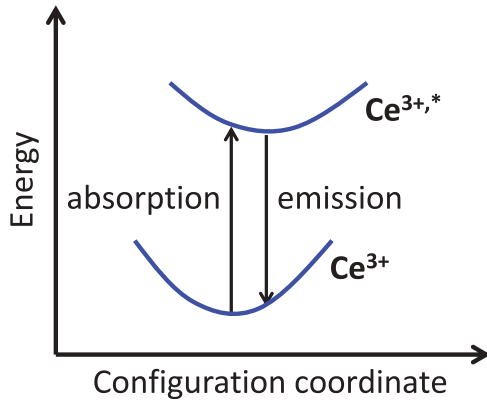
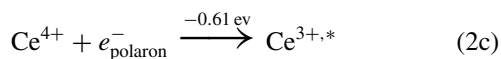
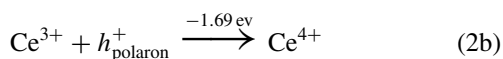


FIG. 6. (Color online) Configuration coordinate diagram of the optical (vertical) transition of Ce^{3+} to excited $\text{Ce}^{3+,*}$ and the emission from $\text{Ce}^{3+,*}$. See the text for the calculated and experimental absorption/emission energies.



The absorption energy for the Ce^{3+} ion and the emission energy for the excited $\text{Ce}^{3+,*}$ ion are calculated to be 3.86 and 3.71 eV, respectively, by taking the energy difference between $\text{Ce}^{3+,*}$ and Ce^{3+} . This is illustrated in Fig. 6, where absorption energy is calculated using the relaxed structure of Ce^{3+} while emission energy is calculated using the relaxed structure of $\text{Ce}^{3+,*}$. In comparison, experimentally observed optical absorption by Ce in $\text{Cs}_2\text{LiYCl}_6$ exhibits a broad band centered at 3.7 eV, while the Ce 5d to 4f emission has two peaks centered at 3.35 and 3.06 eV.¹⁷ Splitting is due to spin-orbit splitting of the Ce 4f band. The calculation for Ce^{4+} , including spin-orbit coupling, indeed shows splitting of the 4f band in Fig. 5(b) by 0.34 eV. The calculated Ce absorption energy is in good agreement with the experimental value. The proximity of STE emission energy and Ce absorption energy enables radiative energy transfer from the STEs to Ce^{3+} ions. The calculated Ce emission energy is somewhat larger than the experimental value, perhaps because of the errors in excited-state structural relaxation.

IV. DISCUSSION

A. Carrier transport in elpasolites

To our knowledge, all elpasolite compounds that have been investigated as scintillators are rare-earth elpasolites. Because rare-earth elements are typically more electronegative than alkali metal elements on A and B sites, the localized *d* or *f* states of the rare-earth cations are expected to form the conduction band edge states. These states are further localized by the large distance between the rare-earth cations, as dictated by the double-perovskite structure of elpasolites. Therefore, the narrow conduction band with small dispersion, similar to that of $\text{Cs}_2\text{LiYCl}_6$, is expected for many other rare-earth elpasolites. Indeed, our calculations found this result for other

rare-earth elpasolites, such as $\text{Cs}_2\text{NaLaCl}_6$.³⁸ This means that relatively slow scintillation as a result of inefficient carrier transport to activators may be a general phenomenon for many rare-earth elpasolites, especially for chlorides. The exception may be that the A- or B-site cation (typically alkali metal elements) is replaced by more electronegative cations, which form more delocalized conduction band edge states. In general, using less electronegative anions should improve the hole transport efficiency and using more electronegative cations should improve the electron transport efficiency. Both approaches should also reduce the band gap. Faster carrier transport should lead to faster scintillation response, and a small band gap may increase the light yield.

B. PBE0 versus HSE06

We now compare PBE0 and HSE06 results on the band gap and the Ce impurity in $\text{Cs}_2\text{LiYCl}_6$. The PBE0 band gap of 7.08 eV is larger than the HSE06 band gap of 6.34 eV and is closer to the experimentally estimated band gap of 7.5 eV.¹⁷ The band offsets between PBE0 and HSE06 results are calculated by assuming a common reference energy in the two calculations, i.e., the average electrostatic potential in the supercell, and the results are shown in Fig. 7. The hole trapping energy level for Ce^{3+} , $\varepsilon(0/+)$, and the electron trapping energy level for Ce^{4+} , $\varepsilon(0^*/+)$, are also shown in Fig. 7. Here, $\varepsilon(0^*/+)$ is associated with trapping of an electron at the Ce 5d level, resulting in an excited state of $\text{Ce}^{3+,*}$. The hole and electron trapping levels are shallower with respect to the band edges in the HSE06 calculations but are closely aligned with the PBE0 results in the absolute scale. Accurate determination of the band edges is key to the calculations of the carrier trapping levels. Because the PBE0 calculation produces a band gap closer to the experimental value than does the HSE06 calculation, we used PBE0 results throughout this paper. The trapping energy levels shown in Fig. 7 are related to the trapping of free carriers, different from the trapping of polarons discussed in Sec. III C. The differences are simply the polaron binding energies. In $\text{Cs}_2\text{LiYCl}_6$, free carriers are unstable against the formation of polarons.

As discussed in Sec. III C, the absorption energy for the Ce^{3+} ion and the emission energy for the excited $\text{Ce}^{3+,*}$ ion

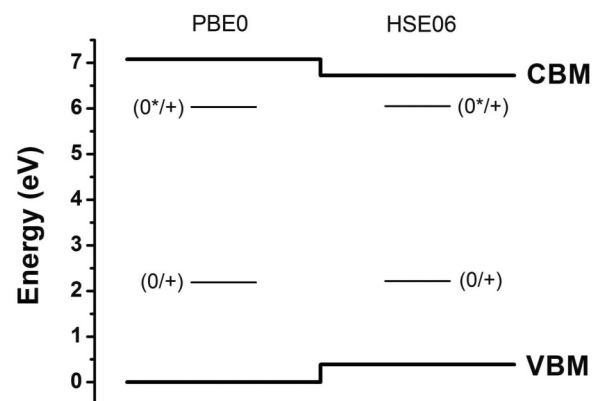


FIG. 7. The hole trapping energy level for Ce^{3+} , $\varepsilon(0/+)$, and the electron trapping energy level for Ce^{4+} , $\varepsilon(0^*/+)$, calculated using PBE0 and HSE06 functionals.

are calculated to be 3.86 and 3.71 eV, respectively, using PBE0 functionals. The HSE06 results are 3.91 and 3.76 eV, respectively, close to the PBE0 results. The energy differences between the empty $4f$ and the empty $5d$ states of Ce^{4+} calculated using PBE0 and HSE06 functionals are nearly the same: 3.15 eV (PBE0) vs 3.16 eV (HSE06). Similarly, the PBE0 and HSE06 results on the $4f$ - $5d$ gap of Ce^{4+} in CeO_2 are close to each other.³⁹ Adding one electron to the $4f$ level to form Ce^{3+} or to the $5d$ level to form $Ce^{3+,*}$ lowers the energy of the occupied level more in the PBE0 calculation than in the HSE06 calculation due to the larger correction of the self-interaction error in the PBE0 calculation. The Ce absorption and emission energies are the energy differences between Ce^{3+} and $Ce^{3+,*}$. The discrepancies between PBE0 and HSE06 results of Ce^{3+} and $Ce^{3+,*}$ are largely canceled out when taking the energy difference of Ce^{3+} and $Ce^{3+,*}$. Thus, the absorption and emission energies for the Ce ion calculated using PBE0 and HSE06 are close to each other.

V. CONCLUSIONS

We have studied the electronic structure, the formation of polarons and STEs, and the carrier trapping at Ce impurities in Cs_2LiYCl_6 , a prototypical elpasolite scintillator with potential

applications in room-temperature radiation detection. We found that slow scintillation in Cs_2LiYCl_6 and many other rare-earth elpasolites should be related to localized electronic states in both valence and conduction bands, causing self-trapping of both holes and electrons and the formation of small polarons and strongly bound STEs. Carrier transport in Cs_2LiYCl_6 should be in the form of slow hopping of STEs and polarons. This hinders carrier transport to Ce ions, where the trapped electrons and holes can recombine radiatively. The proximity of calculated STE emission energy and Ce absorption energy confirms experimentally observed radiative energy transfer from STEs to Ce ions. These results suggest that energy may transfer from radiation-generated charge carriers to Ce ions via a combination of radiative and nonradiative channels. Both should be slow, because the former is limited by the lifetime of the self-trapped triplet excitons while the latter is limited by the slow hopping of the STEs and polarons.

ACKNOWLEDGMENTS

We are grateful for stimulating discussions with David J. Singh and Pieter Dorenbos. This work was supported by the US Department of Energy's Office of Nonproliferation Research and Development NA22.

*mhdu@ornl.gov

¹P. A. Rodnyi, *Physical Processes in Inorganic Scintillators* (CRC Press, Boca Raton, FL, 1997).

²K. S. Song and R. T. Williams, *Self-Trapped Excitons* (Springer-Verlag, Berlin, 1996).

³P. Dorenbos, *Phys. Status Solidi A* **202**, 195 (2005).

⁴M. D. Birowosuto and P. Dorenbos, *Phys. Status Solidi A* **206**, 9 (2009).

⁵A. Canning, A. Chaudhry, R. Boutchko, and N. Grønbech-Jensen, *Phys. Rev. B* **83**, 125115 (2011).

⁶J. Glodo, E. van Loef, R. Hawrami, W. M. Higgins, A. Churilov, and K. S. Shah, *IEEE Trans. Nucl. Sci.* **58**, 333 (2011).

⁷W. M. Higgins, J. Glodo, U. Shirwadkar, A. Churilov, E. van Loef, R. Hawrami, G. Ciampi, C. Hines, and K. S. Shah, *J. Cryst. Growth* **312**, 1216 (2010).

⁸J. Glodo, W. M. Higgins, E. van Loef, and K. S. Shah, *IEEE Trans. Nucl. Sci.* **56**, 1257 (2009).

⁹J. Glodo, W. M. Higgins, E. V. D. van Loef, and K. S. Shah, *IEEE Trans. Nucl. Sci.* **55**, 1206 (2008).

¹⁰A. Bessière, P. Dorenbos, C. W. E. van Eijk, K. W. Krämer, and H. U. Güdel, *IEEE Trans. Nucl. Sci.* **51**, 2970 (2004).

¹¹J. Glodo, E. V. D. van Loef, W. M. Higgins, and K. S. Shah, *IEEE Nuclear Science Symposium Conference Record*, Vol. N30-164, pp. 1208 (IEEE, New York, NY, 2006).

¹²M. D. Birowosuto, P. Dorenbos, J. T. M. de Hass, C. W. E. van Eijk, K. W. Krämer, and H. U. Güdel, *IEEE Trans. Nucl. Sci.* **55**, 1152 (2008).

¹³G. Rooh, H. J. Kim, and S. Kim, *IEEE Trans. Nucl. Sci.* **57**, 1255 (2010).

¹⁴A. Bessière, P. Dorenbos, C. W. E. van Eijk, K. W. Krämer, H. U. Güdel, and A. Galtayries, *J. Lumin.* **117**, 187 (2006).

¹⁵G. Rooh, H. J. Kim, and S. Kim, *Radiat. Meas.* **45**, 412 (2010).

¹⁶E. V. D. van Loef, P. Dorenbos, C. W. E. van Eijk, K. W. Krämer, and H. U. Güdel, *J. Phys. Condens. Matter* **14**, 8481 (2002).

¹⁷A. Bessière, P. Dorenbos, C. W. E. van Eijk, L. Pidot, K. W. Krämer, and H. U. Güdel, *J. Phys. Condens. Matter* **16**, 1887 (2004).

¹⁸P. Yang, F. P. Doty, M. A. Rodriguez, M. R. Sanchez, X. Zhou, and K. S. Shah, *Materials Research Society Symposium Proceedings*, pp. 1164-L11-05 (Materials Research Society, 2009).

¹⁹M. D. Birowosuto, P. Dorenbos, C. W. E. van Eijk, K. W. Krämer, and H. U. Güdel, *J. Phys. Condens. Matter* **18**, 6133 (2006).

²⁰G. Meyer, *Prog. Solid State Chem.* **14**, 141 (1982).

²¹Th. Pawlik and J.-M. Spaeth, *J. Phys. Condens. Matter* **9**, 8737 (1997).

²²K. S. Shah, J. Glodo, M. Klugerman, W. W. Moses, S. E. Derenzo, and M. J. Weber, *IEEE Trans. Nucl. Sci.* **50**, 2410 (2003).

²³G. Kresse and J. Furthmüller, *Phys. Rev. B* **54**, 11169 (1996).

²⁴G. Kresse and D. Joubert, *Phys. Rev. B* **59**, 1758 (1999).

²⁵J. P. Perdew, M. Ernzerhof, and K. Burke, *J. Chem. Phys.* **105**, 9982 (1996).

²⁶G. Kresse and J. Furthmüller, *Phys. Rev. B* **54**, 11169 (1996).

²⁷J. Heyd, G. E. Scuseria, and M. Ernzerhof, *J. Chem. Phys.* **118**, 8207 (2003).

²⁸J. Heyd, G. E. Scuseria, and M. Ernzerhof, *J. Chem. Phys.* **125**, 224106 (2006).

²⁹J. Paier, M. Marsman, K. Hummer, G. Kresse, I. C. Gerber, and J. G. Angyan, *J. Chem. Phys.* **124**, 154709 (2006).

³⁰K. Biswas and M.-H. Du, *Appl. Phys. Lett.* **98**, 181913 (2011).

³¹M.-H. Du, *J. Appl. Phys.* **108**, 053506 (2010).

³²M.-H. Du and S. B. Zhang, *Phys. Rev. B* **80**, 115217 (2009).

- ³³P. E. Blöchl, *Phys. Rev. B* **50**, 17953 (1994).
- ³⁴G. Kresse and D. Joubert, *Phys. Rev. B* **59**, 1758 (1999).
- ³⁵C. Reber, H. U. Gudel, G. Meyer, T. Schleid, and C. A. Daul, *Inorg. Chem.* **28**, 3249 (1989).
- ³⁶A. L. Shluger and A. M. Stoneham, *J. Phys. Condens. Matter* **5**, 3049 (1993).
- ³⁷A. M. Stoneham, J. Gavartin, A. L. Shluger, A. V. Kimmel, D. Muñoz Ramo, H. M. Rønnow, G. Aeppli, and C. Renner, *J. Phys. Condens. Matter* **19**, 255208 (2007).
- ³⁸M.-H. Du, (unpublished).
- ³⁹J. L. F. Da Silva, M. V. Ganduglia-Pirovano, J. Sauer, V. Bayer, and G. Kresse, *Phys. Rev. B* **75**, 045121 (2007).